NASA Technical Memorandum 81662

# Experimental Analysis of IMEP in a Rotary Combustion Engine



H. J. Schock, W. J. Rice,
and P. R. Meng
*Lewis Research Center*
*Cleveland, Ohio*


Prepared for the
International Symposium of the Society of
Automotive Engineers
Detroit, Michigan, February 23-27, 1981

NASA

# EXPERIMENTAL ANALYSIS OF IMEP IN A ROTARY COMBUSTION ENGINE

by H. J. Schock, W. J. Rice and P. R. Meng

National Aeronautics and Space Administration
Lewis Research Center
Cleveland, Ohio 44135

## SUMMARY

This experimental work demonstrates the use of a NASA designed, real time Indicated Mean Effective Pressure (IMEP) measurement system which will be used to judge proposed improvements in cycle efficiency of a rotary combustion engine. This is the first self-contained instrument that is capable of making real time measurements of IMEP in a rotary engine. Previous methods used require data recording and later processing using a digital computer. The unique features of this instrumentation include its ability to measure IMEP on a cycle by cycle, real time basis and the elimination of the need to differentiate the volume function in real time.

Measurements at two engine speeds (2000 and 3000 RPM) and a full range of loads are presented, although the instrument was designed to operate to speeds of 9000 RPM.

THE ROTARY ENGINE is of interest as a future powerplant for general aviation aircraft because of its advantages in simplicity, compactness, high specific power, stratified charge adaptability and low noise levels. The main disadvantage of rotary engines is that they have a 12% higher specific fuel consumption (SFC) than do comparable reciprocating engines according to work recently completed under a NASA contract (1)*. In an aircraft, the advantages of high specific power together with the multifuel tolerance of the rotary engine may outweigh the apparent disadvantage in SFC.

To evaluate potential performance and economy gains that might be realized by further development of the rotary engine, a research program aimed at quantifying these possible gains was begun at NASA Lewis Research Center. It was decided that in order to evaluate potential gains and determine where losses occurred, basic measurement such as IMEP were necessary.

The need to make IMEP measurements has long been recognized and much discussed. Brown (2,3) presented an extensive analysis on the measurements and interpretation of IMEP measurements in both direct injection and prechamber diesel engine. Brown's approach uses two analog signals that represent pressure and volume; analog circuits operate on these signals and produce an output voltage proportional to IMEP. Brown considered using digital circuitry but felt at the time that these circuits were not fast enough to give good detail and thus good accuracy. In later work, Lancaster et al (4) describes a procedure for measuring IMEP by averaging a digitized pressure signal at one crank angle. With this type of system, as with the method described by Brown, analysis of cycle-to-cycle variability and the causes of this variability are not possible as events within a cycle may be obscured by this averaging.

*Numbers in parenthesis designate References at end of paper.

Researchers at NASA LeRC have been making real time IMEP measurements in piston engines for several years. Rice and Cassidy (5) have been able to observe above mean values of IMEP in a cycle following a below mean value of IMEP. This was attributed to the higher concentration of unburned fuel in the residual gases from the first cycle, making the charge of the second cycle more fuel-rich.

Attempts at identification of the causes of this cycle to cycle variability are underway by many researchers. It is known that mixing and turbulence directly affect cycle to cycle variability, but the exact form of this relationship is complex and unknown. It will be especially important to quantify these variations as stratified charge engine development progresses.

Several attempts have been made to measure IMEP in a rotary engine (6,7,8) but all have involved post run processing of collected data. One of the disadvantages to this method is that considerable periods of time may be spent collecting data that is defective before the researcher is aware of the erroneous results. The objective of this investigation was to develop a system to measure IMEP on a cycle-by-cycle, real-time basis. The instrument could then be used to assess efficiency improvements associated with changes in engine variables such as combustion chamber geometry, seal changes, and intake and exhaust manifold configuration without additional post-test data processing. In addition, because of its real time computational ability, this instrument could be used for engine control purposes.

## STATEMENT OF PROBLEM

This experimental work was conducted to demonstrate the performance of an IMEP measurement system for use in a rotary combustion engine. Figure 1 is a graphic representation of how the rotor moves within the epitrochoidal shaped housing for a complete engine cycle. For the Wankel type rotary engine, a thermodynamic cycle consists of 1080 crank angle degrees. These pictoral representations were produced via computer code

developed as part of this work. The equations which describe the housing profile and rotor motion were taken from Ansdale (9). As this figure shows, in order to follow the pressure in a thermodynamic system of interest throughout the cycle, either a transducer must be mounted on the rotor face or a series of transducers located in the housing must be electronically switched to follow the rotor face throughout the cycle. The system chosen is the latter method and it uses four piezoelectric transducers located as shown. The unique feature of this instrumentation is its ability to compute and display IMEP on a cycle by cycle, real-time basis.

## EQUIPMENT AND TEST PROCEDURE

The test rig used for these experiments is shown in Figure 2. A 1978 Mazda 12A non-emission type engine rated at 82 KW (110 BHP) @ 7000 RPM was used. The two rotor engine has a displacement of 1.15 liters (70 $in^3$) and a 9.4:1 compression ratio. This engine was chosen as it represents an inexpensive testbed for instrument development compared to available alternatives. In addition, it couples a late version of apex seal technology with an advanced combustion chamber design (10) to produce an engine with high specific power and good fuel economy relative to previous rotary engines. This engine is the same model as that used by Danieli (8).A four speed manual transmission was utilized to couple the engine to a 250 HP dynamometer. Motoring of the engine was accomplished with a 25 HP constant speed (1770 RPM), motor located on the dynamometer. The engine was capable of being motored at several speeds by using various combinations of belt-driven pulleys between the motor and dynamometer. Transmission gearing provided additional flexibility in choosing the desired engine speeds.

Complete conventional instrumentation was installed on the engine in addition to the special combustion instrumentation which will be discussed in detail later in this report. Automatic control systems were utilized for engine speed, dynamometer load, and coolant

discharge temperature. Load was measured both with a reaction load cell and a Lebow Associate Torquemeter model 1604-2K which was installed between the dynamometer and the transmission as shown in Figure 2. An optical shaft angle encoder was installed on the front of the engine and was belt driven at a 3:2 ratio by the eccentric shaft.

Exhaust emissions were measured by a Scott Research Laboratories Test Console which incorporated the following equipment:

A Scott Total Hydrocarbon Analyzer Model 415

A Scott Model 250 $O_2$ Analyzer

A Scott Model 125 $NO/NO_x$ Analyzer

A Beckman Model 864 $CO_2$ Analyzer

A Beckman Model 865 CO Analyzer

Engine operation was monitored on the alpha-numeric CRT displays in the the control room. A micro-processor at the test cell was utilized to interface with a central minicomputer which performed on line calculations and continuously updated the CRT displays. An IBM-3033 was used for necessary post-run processing and graphical analysis of collected data.

The engine was operated at steady state conditions (speed, load and water temperature), at which time the data were recorded and oscilloscope traces were photographed. Steady state was said to exist when there was agreement of $\pm$ 5% between the air fuel (A/F) ratio from the direct measurement of air flow and fuel flow and the A/F ratio calculated from the method of Spindt. The dynamometer motor was then started and allowed to come up to the engine speed. At this point the fuel was cut off to the engine. After allowing a short time for stabilization, the motoring data were recorded while the engine was still at normal operating temperature.

## DEFINITION AND BASIC EQUATIONS

In this work, the following definitions have been used. The subscript "F" indicates firing, "M" indicates motoring and "D" indicates the quantity was back calculated from a torque and speed measurement.

$$IMEPT = \oint PdV/V_d = IMEP + PMEP$$

IMEP - Indicated mean effective pressure (Fig. 3)

PMEP - Pumping mean effective pressure (Fig. 3)

FMEP - Friction mean effective pressure

BMEP - Brake mean effective pressure

MMEP - Motoring mean effective pressure

BHP - Brake Horsepower

The calculation of BMEP and MMEP for the rotary engine follows from the classical definition of brake mean effective pressure in any positive displacement engine. That is the theoretical constant pressure exerted during each powerstroke of the engine to produce the observed work output, assuming no losses.

For a positive displacement rotary engine:

$$\frac{\text{Work}}{\text{Stroke}} * \frac{\text{Strokes}}{\text{Min}} = \text{Power Out} \qquad (1)$$

$$\frac{(BMEP * V_d)\ \text{in-lb}_f}{(12\ \text{in/ft})} * \frac{N}{x} = BHP \quad \frac{(33000\ \text{ft-lb}_f)}{\text{min Hp}} \qquad (2)$$

$$BMEP = \frac{(BHP)\ (12)\ (33000)\ x}{V_d\ (N)} \qquad (3)$$

$V_d$ = Volume displaced during power stroke

N = Speed of power shaft, RPM

x = Number of revolutions required for the work ($V_d$ * BMEP) to be delivered.
x = 1 for this engine

The calculation of MMEP follows directly.

The following equality can now be written.

$$BMEP_{D,F} = IMEP_F + PMEP_F - FMEP_F \quad (4)$$

$PMEP_F$ is a negative quantity for this naturally aspirated engine.

Assuming $FMEP_F = FMEP_M$

$$FMEP_F = MMEP - \left(\oint \frac{P_d V}{V_d}\right)_M \quad (5)$$

The objective of motoring the engine is to determine $FMEP_M$. The standardized work input, MMEP, consists of the following parts:

$PMEP_M$ - Pumping Work (neg term)

$FMEP_M$ - Engine Friction (neg term)

$QMEP_M$ - Heat Transfer Losses (neg term)

For the rotary engine QMEP is a significant factor in this calculation and is included in it as it represents work lost by means other than engine friction.

One can then use the following equality to determine if this direct measurement corresponds to the back calculated value.

$$\left(\oint \frac{P_d V}{V_d}\right)_f = BMEP - MMEP + \left(\oint \frac{P_d V}{V_d}\right)_M \quad (6)$$

The instrument system described in this report can measure the following quantity in either the motoring or firing configuration.

$$\oint \frac{P_d V}{V_d} = IMEP + PMEP \quad (7)$$

It can also be used to measure only the IMEP or only the PMEP in either the motoring or firing configuration.

REAL TIME IMEP MEASUREMENT SYSTEM

PRESSURE TRANSDUCERS - This instrument system has been designed to be used with four transducers that are sequentially switched in synchronization with the rotor rotation. Since a rotor face spans a $120^0$ sector, at least three transducers are required. Because of geometric restrictions and the desire to have an overlap region, it is more practical to use four transducers.

Piezoelectric transducers were used because of their high frequency response and good high temperature performance. However, this type of transducer has no inherent reference point and tends to have a high output offset drift with time and temperature.

The individual transducers are located in the rotor housing in such a manner that there is physical overlap by the rotor of two successive transducers (leading and trailing) for a brief period prior to switching. During this overlap period the average difference between the two transducers is measured and is used to offset the trailing transducer. Thus, when the correlator switches from the leading transducer to the trailing transducer a continuous waveform is produced. The difference averaging circuitry is unique in that the averaging period is a function of the rotor angle only and is thus independent of engine RPM. Operation of the signal correlator extends to 9000 engine RPM (3000 rotor RPM), and a comprehensive description of its operation is given in Appendix A.

The physical location of the pressure transducers is shown in Figure 4. Transducers 1, 2, and 3 are Kistler Model 601B and are cooled by the engine water jacket cooling system. Transducer number 4 is located in the exhaust manifold just downstream of the exhaust exit on the rotor housing. Temperature of this transducer was maintained by a water-cooled copper wrap around the transducer holder.

Flush mounted water cooled transducers would have been a more acceptable installation, but the primary objective of this work was to demonstrate the feasibility of using

the system described. Geometrical constraints which would have made extensive rotor housing modification necessary did not seem appropriate for proof of this concept.

The sensitivity of piezoelectric transducers changes with temperature, and thus it was necessary to determine their operating temperatures. To do this, four transducers were drilled and fitted with thermocouples as shown in Figure 5. The thermocouples were placed as close as possible to the diaphragm of the transducer. Tests were then conducted at loads varying from 20 to 100 ft-$lb_f$ and speeds of 1000 to 5000 RPM to determine the temperature at which the transducers would operate.

Based on the results of the temperature data each of the transducers installed had the sensitivity of its charge amplifier adjusted to compensate for the temperature at which it would operate. At 180° F coolant temperature, the average temperature that the three transducers in the housing operated was 193.1° F. The average temperature of the transducer in the exhaust manifold was 73.5° F. Spot checks of transducer temperatures while motoring the engine, which was done in each case immediately after firing, showed little deviance from the firing temperatures. All measured temperatures are within the operating limits prescribed by the transducer manufacturer (11).

SIGNAL CORRELATOR AND SHAFT ANGLE ENCODER - The Signal Correlator was designed to take these four pressure transducer signals and produce one composite continuous pressure waveform for the P-V diagram analysis.

The outputs from the pressure transducer are signal-conditioned by Kistler Model 504E charge amplifiers. The outputs of the charge amplifiers are connected to the four inputs of the signal correlator marked P1, P2, P3, and P4 (Figure 6). The composite pressure waveform is available at the P-OUT jack.

An absolute position optical shaft angle encoder is used to provide rotor angle information to the signal correlator. The encoder is belt-driven from the engine output shaft with a 3:2 ratio. Thus, for every three out-

put shaft revolutions, the encoder turns two revolutions and the rotor, by virtue of internal gearing, turns one revolution. The 3:2 encoder drive ratio was chosen so that one engine combustion cycle would be represented by 720° of encoder rotation as is the case for a four cycle piston engine. This allows additional NASA-developed instrumentation to be used without special modification for this engine (12).

The encoder resolves to 0.35° at its own shaft which translates to 0.53° engine output shaft rotation, and 0.18° rotor rotation. The active regions and the transition (overlap) regions are shown in Figure 7 referenced to encoder rotation. The 0° encoder rotation reference point is chosen such that the volume of the combustion chamber being investigated is at the minimum volume position (non-firing).

Figure 8 shows (clockwise from upper left): (a) the four individual pressure transducer signals versus crank angle for one cycle where top dead center (TDC) is defined as the minimum volume condition and bottom dead center (BDC) as the maximum volume condition so as to be analogous to the piston engine; (b) the composite pressure signal, pieced together and vertically aligned for rotor face A for one cycle; (c) the resultant pressure-volume diagram displayed on an oscilloscope using the composite pressure signal; (d) a 10 times expansion of the P-V diagram to better illustrate the pumping loop; and, (e) a p-θ blowup of the transducer overlap region.

Examination of the 10x expansion of pumping loop in Figure 8 shows a pressure rise approximately midway through the exhaust stroke. Further investigation shows that this pressure rise began when the second rotor reached the exhaust port. It is believed that separate exhaust manifolds would have eliminated this rise and a 2% increase in work out would have been realized at this speed and load.

The presence of a passage between the housing and the pressure transducer diaphragm presents an additional complication in interpreting the observed pressure signal. Three

such distortions were described by Evers (13). They are: phase error due to lag time, frictional pressure loss, and a distortion caused by response. No attempt was made to correct for these errors. Oscillatory pressures were observed and are shown in Figure 8E. The question arises as to whether this oscillation is caused by a pressure wave in the combustion chamber or in the passage of the transducer. Using the equation proposed by Sears and Zemansky (14) the resonant frequency, $F_R$, of this passage length was calculated for test point No. 1 as follows:

$$F_R = \frac{C}{4L} \qquad (8)$$

L = Characteristic length of passage.
C = Speed of sound @ temp of the gas.

The temperature was assumed to be equal to the temperature of the diaphragm, 183° F. Assuming the gas in the passage is a perfect gas, the speed of a wave can be estimated from;

$$C = \sqrt{\gamma g_c RT} \qquad (9)$$

@ 180° F , $C \cong 1243$ ft/sec

$\therefore F_R = 5736$ Hz

The trace on the photograph (Fig. 8E) oscillates at about 5250 Hz which leads one to believe that the observed oscillation is in the transducer passage. It is also interesting to note that in this overlap region the gas in both transducer passages appears to be oscillating at the same frequency. This is to be expected as the gas temperature and tube length are approximately the same in each of the two passages.

IMEP INSTRUMENT - The IMEP instrument evaluates the $\int PdV$ in the crank angle domain as follows:

$$\frac{1}{V_d}\oint P_d V = \frac{1}{V_d}\int_0^{6\pi} P \left(\frac{dV}{d\theta}\right) d\theta \qquad (10)$$

= Crank angle degrees

In this form the function dV/dθ can be determined from the engine geometry and does not need to be computed in real time. This function is stored in the instrument in read-only memory (ROM). A plot of dV/dθ vs. θ for the engine is shown in Figure 9.

The basic operation of the system is illustrated in the block diagram of Figure 10. Engine crank angle data is generated external to the instrument by an absolute shaft angle encoder. This crank angle data is input to a Memory Address Decoder (MAD). The MAD generates the actual memory address, sign of the computation and the computation start and stop signals. The 256 values of dV/dθ starting at bottom dead center (BDC) and ending at top dead center (TDC) are preprogrammed and stored in Read Only Memory (ROM). Because of the symmetry in the volume crank angle relationship for the rotary engine, the values of dV/dθ from TDC to BDC are the negative of those from BDC to TDC for equal angles before and after TDC. Therefore, only the magnitude of dV/dθ is stored in the ROM. This effectively increases the resolution of a fixed memory word size unit by a factor of 2. In addition, it allows the Multiplying Digital to Analog Converter (MDAC) and the Analog to Digital Converter (ADC) to be unipolar devices, thus eliminating any errors due to zero effects and zero drift with time or temperature.

The contents of the ROM are applied as the digital input to a multiplying or scaling digital to analog converter (MDAC). The pressure signal from the correlator is applied as an analog input to the MDAC.

The output of the MDAC is an analog signal equal to the product P(dV/dθ). The signal is then digitized by the ADC.

The computation of IMEPT is performed according to the approximation:

$$\oint \frac{P dV}{V_d} \cong K \sum_{0}^{1023} P \left(\frac{dV}{d\theta}\right) \quad d\theta \qquad (11)$$

where K = scaling constant.

Figure 11 shows a PV diagram for a typical computation of p(dV/dθ). The computational slices contain the following terms:

From the intake stroke: $P_1 V = A1$

From the compression stroke: $- P_3 V = - (A3 + A2 + A1)$

From the power stroke: $P_4 V = + (A4 + A3 + A2 + A1)$

From the exhaust stroke: $P_2 V = - (A2 + A1)$

Collecting terms yields the slice sum: $A4 - A2$

The terms on the compression and exhaust stroke are treated as negative in the computation, since $(dV/d\theta)$ is negative in these regions.

The $\Delta V$ slices vary in width since the computation is performed at constant $\Delta\theta$ increments. Thus, the slices are more numerous and of smaller width in the regions of TDC and BDC. This is fortuitous as the region of steepest pressure gradients would normally occur at these locations.

In addition to the signal correlator additional instruments were used to measure peak pressure and angle of peak pressure. A bargraph generator was also used to display 100 consecutive cycles of IMEPT, $PMEP_F$, peak pressure and angle of peak pressure for each test point. The means and standard deviations for these 100 cycle measurements were also computed by this instrument for each test point. Two typical bargraphs are shown in Figure 12A and 12B. Figure 12A shows 100 consecutive cycles obtained in real time using the LeRC signal correlator and IMEP meter while the engine was running at steady speed and load. The upper set of bargraphs on this figure represent 100 consecutive cycles of IMEPT and the lower represents 100 consecutive cycles of PMEP. The second shows the transition of IMEPT from firing to motoring.

RESULTS AND DISCUSSION

Figures 13, 14, and 15 are comparisons of IMEPT calculated from Equation 6 and the same quantity measured directly. The range of

speeds was limited to 3000 RPM (crankshaft) by the motoring capability of our equipment. The measurements were taken at the full range of loads over which the engine will operate for the two speeds tested (see Table 2).

The average difference between the cyclic integral measured and the value of this integral back calculated was 6.0%. In addition to the fact that we are making measurements on only one rotor, there is variability from pocket to pocket on the same rotor. As we did not compute the cyclic integrals of each of the three thermodynamic systems simultaneously, this variability is unknown. The only manner in which a direct comparison could have been made would be to compute the cyclic integral for each of the six systems of interest simultaneously. For combustion analysis, a single rotor engine would be better to use than the multirotor engine as both cost and complexity of the necessary instrumentation would be reduced.

Figure 16 shows that agreement between the measured and back-calculated values of the cyclic integral is poorer at light loads than at higher ones. This may not be surprising because under light-load conditions small differences in rotor-to-rotor power production or system inaccuracies become more pronounced. In addition, the instrumentation is operating at less than 10% of its full scale value at the low-load conditions.

Figure 17 shows how the average coefficient of correlation (Std deviation of IMEPT/Mean IMEPT) varies with power at the two engine speeds tested. This shows that there is more cycle-to-cycle variability at low loads than at moderate and high loads. This phenomenon is generally observed in carbureted engines and is probably due to variations in local air fuel ratios.

Measurements of PMEP were made during firing and motoring at constant intake manifold pressure (IMP). The $PMEP_F$ value should be exactly equal to PMEP motoring at constant IMP and the same speed, if other conditions were equal. All other conditions are not exactly the same as heat transfer to the incoming air fuel charge will be higher in

firing than in the motoring case. This would tend to make the average chamber pressure during intake slightly higher during firing than during motoring and thus reduce PMEP during firing. A comparison of PMEP during firing and PMEP during motoring is shown in Figure 18.

In general, good agreement between these parameters was obtained. The use of a belt-driven motoring device complicated making the motoring measurement in that it was difficult to maintain speed and constant manifold pressure. In addition, the engine came equipped with a carburetor which included a primary and secondary throttle plate. This also made the problem of holding manifold vacuum constant difficult.

In Figure 19 FMEP is shown vs. brake power for the two nominal speeds tested. FMEP is primarily a function of engine speed as would be expected. There is more scatter in the 2000 RPM data than in the 2900 RPM data because variation in PMEP has a smaller effect in the calculation of FMEP (from the MMEP and PMEP measurements) since the frictional term becomes more dominant as the speed increases.

## SUMMARY AND CONCLUSIONS

1. The instrumentation designed to give real time IMEP measurement was built and successfully demonstrated.

2. Cycle-to-cycle variability of the cyclic work integral (IMEPT) expressed as std. deviation/mean, is greater at low loads than at high loads for the rotary engine tested.

3. An accurate determination of engine IMEP will require instrumentation of all the systems that produce work. For a two rotor engine this will be six simultaneous measurements of IMEP.

4. A performance improvement could be realized in this engine by the addition of a second exhaust pipe.

5. PMEP motoring averaged 7% higher than PMEP firing for the conditions tested.

6. The average value of FMEP is 31% higher at 2900 RPM than it is at 2000 RPM.

7. Oscillations in passages do not interfere with the performance of the correlator in a severe manner.

## Appendix A

## CORRELATOR CIRCUIT DESCRIPTION

The circuit diagram for the signal correlator is shown in Figures A1 and A2.

Figure A1 shows the analog signal processing circuitry. This circuitry contains a repetitive circuit block of which the first block is composed of U1, A1, R1, and C1. U1 is a sample-hold amplifier configured as a unity gain inverting summer when the sample switch is closed. When the sample switch is open, the output of U1 is determined by the voltage on capacitor C1. Amplifier A1 is configured as a unity gain inverting summer. Resistor R1 (R1A-R1G) is a laser trimmed thin film resistor network of seven matched resistors. The nominal value of these resistors is 10K $\pm$ 1%, but the seven resistors are matched to 0.1%. One input to U1 is -P1 which is obtained by inverting P1 with amplifier A5. The other input of U1 is P2. Switch S1 is closed periodically during the transition region where both P1 and P2 are reading the combustion pressure. During this time the output of U1 is the instantaneous difference between P1 and P2 ($\Delta 2,1$) when S1 is closed, and the average value ($\overline{\Delta 2,1}$) of this difference when S1 is open. A further discussion of this averaging circuit will follow later in this report. The difference ($\overline{\Delta 2,1}$) is applied as one input to amplifier A1. The other input of A1 is pressure P2. The output of A1 is then:

$$-P2^* = P2 - (P2 - P1)_{AVG.}$$

Thus, P2* is P2 offset by the average difference existing between P2 and P1 during the overlap period where both transducers are reading the same pressure. Hence, the result is to force P2* to equal P1.

The remaining basic circuit blocks function in the same manner. Thus, P3* is forced equal to P2* during the overlap region where P3 and P2 are both active and P4* is forced equal to P3* during their common overlap region. The net result is a continuous pressure waveform with all transducers referenced back to P1.

Any offset drift in the individual transducer signals is cancelled out during each engine cycle. Figure 8A shows the four individual pressure transducer signals versus encoder rotation and Figure 8B shows the composite waveform generated by the signal correlator.

The output of U4 ($\Delta$1,4) is used as an error indicator. Since the transducers are all referenced to P1, the final circuit block should force P1* to equal P1 and $\Delta$1,4 should be zero. If this is not the case, then a gain or sensitivity error is present in one or more of the transducer waveforms. No attempt has been made in the design of the signal correlator to correct for gain errors.

The four signals, -P1, -P2*, -P3*, and -P4*, are applied as the inputs to analog multiplexer, U5. This multiplexer selects one of the four inputs and passes it to amplifier A7, a high input-impedance unity-gain buffer amplifier. Inputs A0 and A1 determine which input signal is selected. Amplifier A7 is used to prevent the multiplexer "ON" resistances from affecting the output. Amplifier A6 is a unity-gain inverting amplifier used to restore the polarity of the input signal.

Figure 12 shows the circuitry used to generate the control signals for the correlator. The major component used for control is an 8 bit by 256 word read-only memory, U7. The address select inputs, A0 through A7, are driven from the shaft angle encoder. The encoder generates digital shaft position signals encoded in a Gray code. This Gray code is partially converted to a complementary natural binary by external circuitry. Additional conversion is performed by exclusive "or" gates U6A and U6B. The resultant code is an 8 bit binary number which specifies the encoder shaft angle in increments of 720°/256 or approximately 2.8°. Because the code is complementary, encoder position 0° is represented by all "one's" and encoder position 720° is represented by all "zeros."

The outputs of U7 are as follows:

A0, A1: Used to select which pressure signal is passed to the P-OUT output.

$\overline{T2,1}$ : Defines the overlap region where both transducers P1 and P2 are active.

$\overline{T3,2}$ : Defines the overlap region where both transducers P2 and P3 are active.

$\overline{T4,3}$ : Defines the overlap region where both transducers P3 and P4 are active.

$\overline{T1,4}$ : Defines the overlap region where both transducers P4 and P1 are active.

The contents of U7 are shown in Table A1 and a timing diagram is shown in Figure A3.

Integrated circuits U8 and U9 are dual one-shot multivibrators. The pulse width for all four one-shots is set at 10 usec. Each one-shot is triggered from a combination of two input signals. One of the inputs is the Tj,i signal from the memory and is used to enable the one-shot only during the respective overlap region. The other input is $\overline{B0}$ which is generated by the shaft encoder. $\overline{B0}$ is the least significant bit of the encoder position and is a square wave signal of period 0.7° (at 6000 encoder RPM, $\overline{B0}$ has a period of 200 sec). Every time $\overline{B0}$ goes from logic "0" to logic "1" a 10 usec negative going pulse is generated by the oneshot if the enabling input (Tj,i) is logic "0". These output pulses are applied as the sample control inputs to the respective sample-hold amplifiers U1 through U4. When the control input is logic "0," the sample switch is closed.

ERROR AVERAGING

When the switch of the sample-hold amplifier is closed, the hold capacitor (C1, C2, C3, or C4) is charged through the respective series resistor. If the switch were closed continuously, then the voltage across the hold capacitor in response to a step input, E, would follow the exponential:

Equation A1 $$E_C = E_{Co} + (E - E_{Co})(1-e^{-t/T})$$

Where $E_C$ = Voltage across the capacitor

$E_{CO}$ = Initial voltage across the capacitor

$t$ = Time

$T$ = Time constant = RC

However, if the switch were closed periodically only for a brief but fixed period of time, t, then the capacitor voltage would follow Equation A1 only during that time. At all other times the capacitor voltage would remain constant at its last value. Therefore, the capacitor voltage is a function of the number of intervals that the switch is closed. If we let:

Equation A2 $\Delta t = T/n$

or

Equation A3 $n\Delta t = T$

$n$ = some fixed number of switch closings

$t$ = period of time the switch is closed

$T$ = time constant

Then from Equation A3 the time constant is proportional to the number, n. Since the number of switch closures is determined by the overlap interval divided by the 80 cycle period, both being independent of RPM, then the filter response or averaging period is RPM independent also.

Having the filter response RPM independent allows maximum utilization of the overlap regions. The hold capacitors are chosen such that 5 time constants are contained in each overlap interval.

Thus, $C_i$ is determined from the following equations:

Equation A4 $5n = \overline{T_{j,i}}/0.7^{o}$

and since:

Equation A5 $n\Delta t = T = RC_i$

Where $T_{j,i}$ = number of degrees in a specific overlap region

$.7^o$ = period of B0 in degrees

n = time constant in sample periods

t = 10 usec.

R = 10,000 ohms

Then substituting Equation A5 into Equation A4 and solving for $C_i$ yields:

Equation A6 $C_i = (\overline{T_{j,i}}/0.7^o)(\Delta t)(1/5R)$

$= \overline{T_{j,i}}\ (10 \times 10^{-6})/(0.7^o)\ (5)\ (10 \times 103)$

$= 286\ \overline{T_{j,i}} \times 10^{-6}$

$C_i$ = Hold capacitor in ufd

$\overline{T_{j,i}}$ = Overlap interval in encoder degrees

From the data in Table A1,

| | | |
|---|---|---|
| $\overline{T_{2,1}}$ | = 110.0° | C1 = 0.31ufd |
| $\overline{T_{3,2}}$ | = 17.0 | C2 = .0049ufd |
| $\overline{T_{4,3}}$ | = 36.0 | C3 = .010ufd |
| $\overline{T_{1,4}}$ | = 14.0 | C4 = .0040ufd |

The closest standard capacitor values to those calculated above were chosen.

## POWER SUPPLY

The signal correlator is packaged for convenience in a Tektronix TM-500 series blank plug-in module kit. The module plugs into a Tektronix Power Module (e.g., RTM 506) which contains the power transformer, rectifiers, filter capacitors, fuses, etc., and also uncommitted NPN and PNP power transistors for use as series pass elements if desired. Figure A2 shows the power supply configuration used in the signal correlator. U11 is a +15 volt, 3 terminal regulator. The input is +33 VDC from the Power Module. C9 is used as a filter capacitor. Similarly, U12 is a -15V regulator with C10 as a filter capacitor. U10 is a +5V regulator which uses one of the external series pass PNP transistors as the series pass element to decrease the current flow through the regulator. C12 is an input filter capacitor and C11 is an output filter capacitor. D1 is a 6.3V zener diode which is used to supply -9 VDC to the memory from the -15 VDC supply.

## CALIBRATION

Because of the use of precision matched gain resistors, no adjustments are needed for gain. The only adjustments are for zero offset. Each sample-hold amplifier has an associated potentiometer for offset adjustment of both the sample-hold amplifier and the associated summing amplifier.

The calibration procedure is as follows:

1. Remove U8 and U9 from their sockets.

2. Ground Pin 4 and Pin 12 of both U8 and U9 sockets. This forces all sample-hold switches to remain closed.

3. Apply a variable DC power supply to input P1 and adjust for -5.000 volts at the output of A5 (-P1).

4. Ground the P2, P3, and P4 inputs.

5. Adjust R6 for a reading of -5.000 volts at the output of A1.

6. Adjust R9 for a reading of -5.000 volts at the output of A2.

7. Adjust R12 for a reading of -5.000 volts at the output of A3.

8. Adjust R15 for a reading of -5.000 volts at the output of A4.

There is no offset adjustment for A5, A7, or A6 because the instruments that use the P-OUT signal have auto-zero functions incorporated in them.

REFERENCES

1. C. Jones, "Multifuel Rotary Aircraft Engine." Paper 801237 presented at AIAA/SAE/ASME 16th Joint Propulsion Conference, Hartford, July 1980.

2. W. L. Brown, "Methods for Evaluating Requirements and Errors in Cylinder Pressure Measurement." Paper 670008, SAE Transactions, Vol. 76, 1967.

3. W. L. Brown, "The Caterpillar IMEP Meter and Engine Friction." Paper 730150, SAE Transactions, Vol. 82, 1973.

4. D. R. Lancaster, R. B. Krieger, and J. H. Lienesch, "Measurement and Analysis of Engine Pressure Data." Paper 750026, SAE Transactions, Vol. 84, 1975.

5. W. J. Rice and J. Cassidy, Internal communication. NASA LeRC, Cleveland, Ohio.

6. M. K. Eberle and E. D. Klomp, "An Evaluation of the Potential Performance Gain From Leakage Reduction in Rotary Engines." Paper 730117, SAE Transactions, Vol. 82, 1973.

7. P. M. Leucht and D. J. Mandley, "Telemetry Applications in the Rotary Combustion Engine." Paper 770877, SAE Transactions, Vol. 86, 1977.

8. G. A. Danieli, J. C. Keck, and J. B. Heywood, "Experimental and Theoretical Analysis of Wankel Engine Performance." SAE Paper 780416, Feb. 1978.

9. R. F. Ansdale, "The Wankel RC Engine," Iliffe, London, 1968.

10. T. Kuroda and H. Satow, "Development on Fuel Economy of Rotary Engine at Toyo Kogyo." October 1979.

11. Kistler, 257-10/73R, "Pressure Sensor and Quartz Engine Pressure Probe, Sundstrand Data Control, Inc.

12. W. J. Rice and A. G. Birchenough, "A Modular Instrumentation System for Real-Time Measurements and Control on Reciprocating Engines." NASA TP-1757, 1980.

13. L. W. Evers, "Spark Plug Transducers for Measuring Indicated Work." SAE Paper 780148, Feb. 1978.

14. F. W. Sears and M. W. Zemansky, "University Physics," 2d. ed., Addison-Wesley, Cambridge, 1955.

## Table 1

### Engine Description

| | |
|---|---|
| Model (MAZDA) | 1978-12A Non-Emissions |
| No. of Rotors | 2 |
| Displacement $in^3/l$ | 70/1.15 |
| Rated BHP at RPM | 110 @ 7000 |
| Compression Ratio | 9.4:1 |
| Ignition | Conventional Breaker Type |

Table 2. Matrix of Test Points
(BHP/KW)

| Nominal Speed | | | | | |
|---|---|---|---|---|---|
| 2046 RF#1 | 10/7.5 | 15/11.2 | 30/22.4 | 35/26.1 | 1, 2, 3, 4 |
| 2046 RF#2 | 10/7.5 | 15/11.2 | 30/22.4 | 35/26.1 | 9, 10, 11, 12 |
| 2046 RF#3 | 10/7.5 | 15/11.2 | 30/22.4 | 35/26.1 | 17, 18, 19, 20 |
| 2950 RF#1 | 10/7.5 | 15/11.2 | 30/22.4 | 45/33.6 | 5, 6, 7, 8 |
| 2950 RF#2 | 10/7.5 | 15/11.2 | 30/22.4 | 45/33.6 | 13, 14, 15, 16 |
| 2950 RF#3 | 10/7.5 | 15/11.2 | 30/22.4 | 45/33.6 | 21, 22, 23, 24 |

*RF = Rotor Face

TABLE A1 - ROM DATA

| Encoder Degrees (To Nearest Whole Degree) | HEX Address | HEX Data |
|---|---|---|
| 00 \| 3 | FF \| FE | F3 \| F3 |
| 6 \| 17 | FD \| F9 | 73 \| 73 |
| 20 \| 115 | F8 \| D6 | F0 \| F0 |
| 118 \| 225 | D5 \| AF | E0 \| E0 |
| 228 \| 329 | AE \| 8A | F1 \| F1 |
| 332 \| 346 | 89 \| 84 | D1 \| D1 |
| 349 \| 515 | 83 \| 48 | F2 \| F2 |
| 518 \| 551 | 47 \| 3B | B2 \| B2 |
| 554 \| 717 | 3A \| 00 | F3 \| F3 |

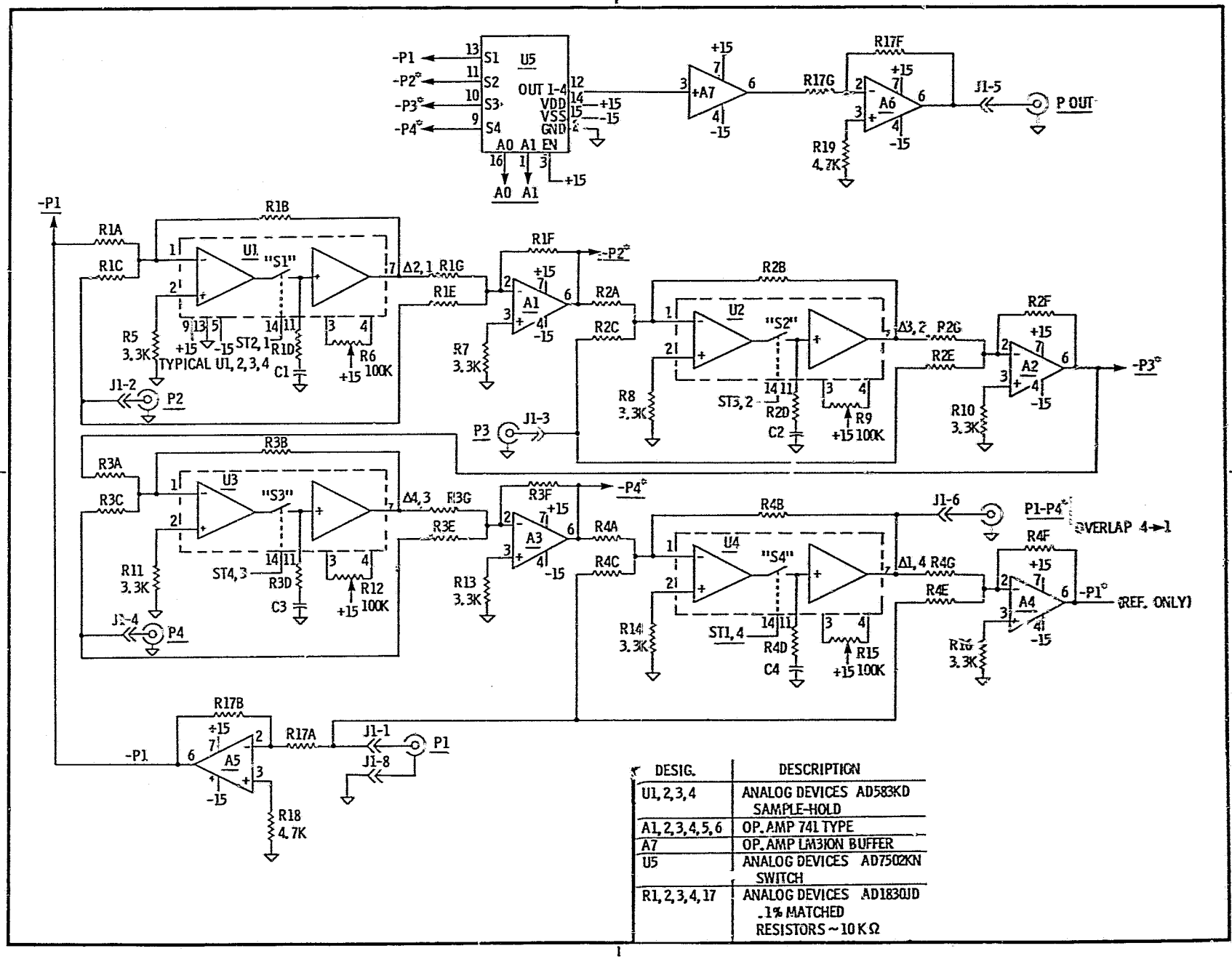


| DESIG. | DESCRIPTION |
|---|---|
| U1, 2, 3, 4 | ANALOG DEVICES AD583KD SAMPLE-HOLD |
| A1, 2, 3, 4, 5, 6 | OP. AMP 741 TYPE |
| A7 | OP. AMP LM310N BUFFER |
| U5 | ANALOG DEVICES AD7502KN SWITCH |
| R1, 2, 3, 4, 17 | ANALOG DEVICES AD1830JD .1% MATCHED RESISTORS ~ 10 KΩ |

Figure A1. - Correlator schematic (analog).

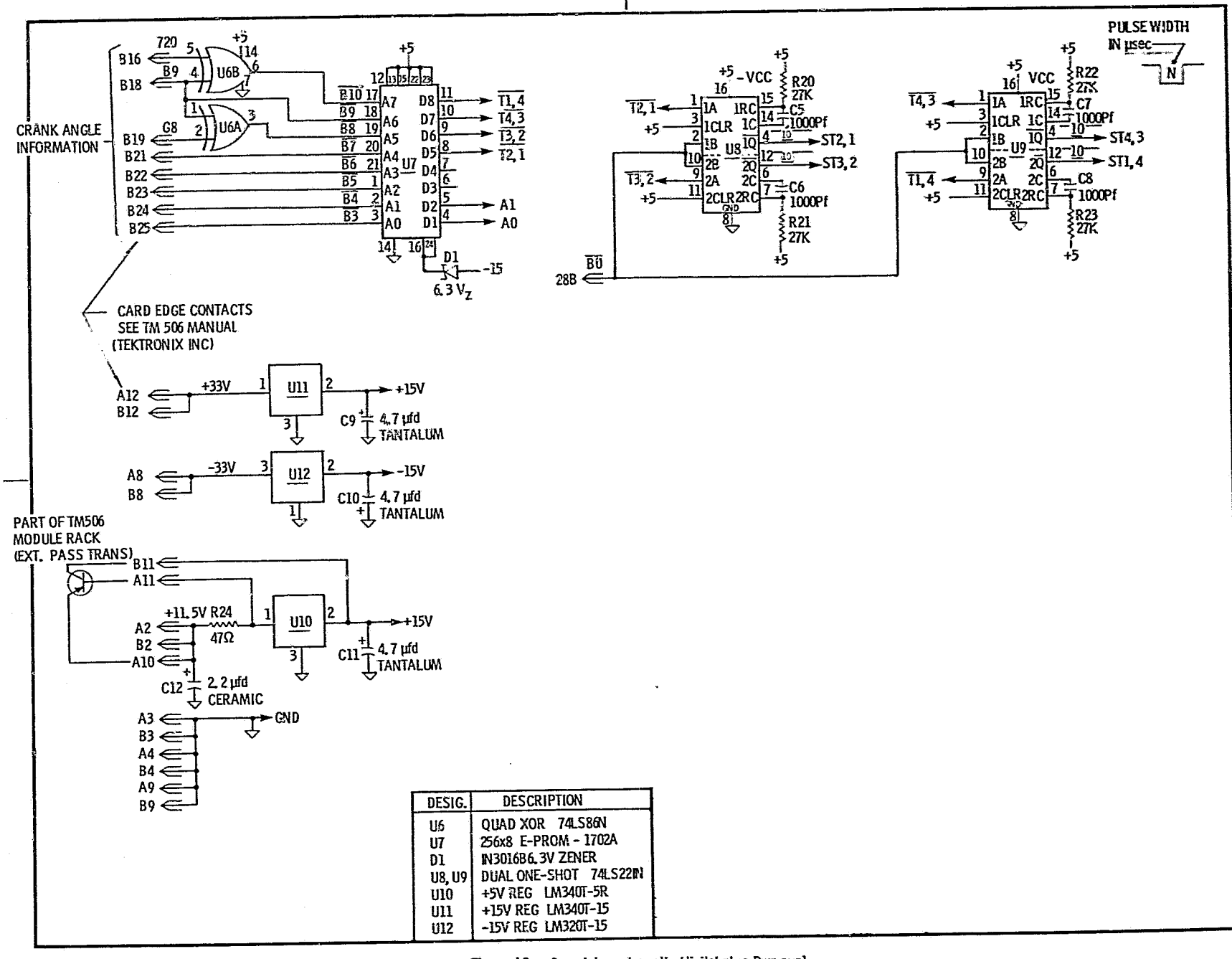


| DESIG. | DESCRIPTION |
|---|---|
| U6 | QUAD XOR 74LS86N |
| U7 | 256x8 E-PROM - 1702A |
| D1 | IN3016B6.3V ZENER |
| U8, U9 | DUAL ONE-SHOT 74LS22IN |
| U10 | +5V REG LM340T-5R |
| U11 | +15V REG LM340T-15 |
| U12 | -15V REG LM320T-15 |

Figure A2. - Correlator schematic (digital plus Pwr sup).

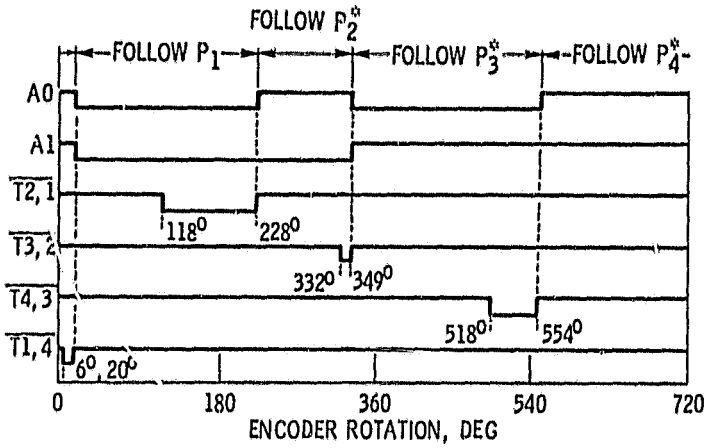


Figure A3. - Timing diagram.

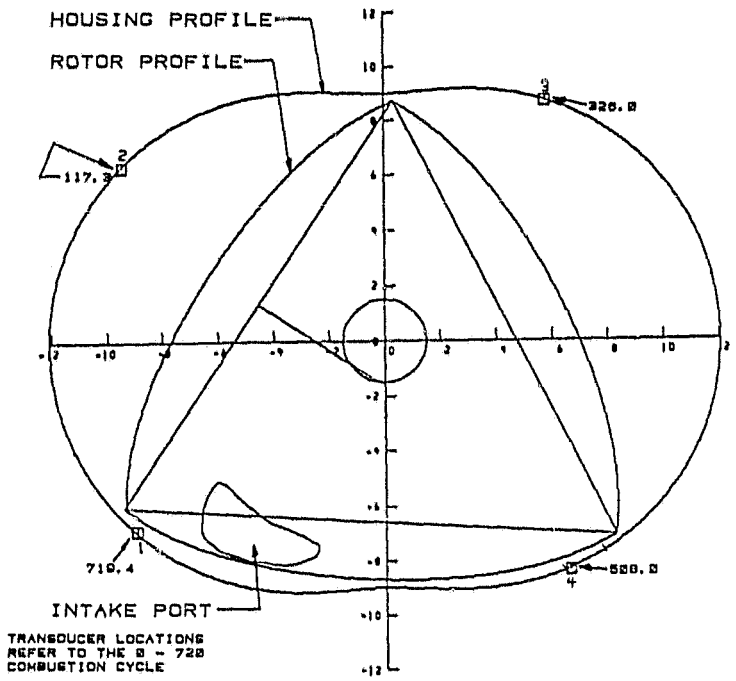


Figure 1A. - Transducer locations.

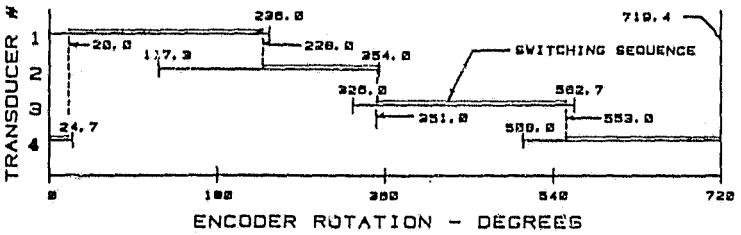


Figure 1B. - Transducer active regions.

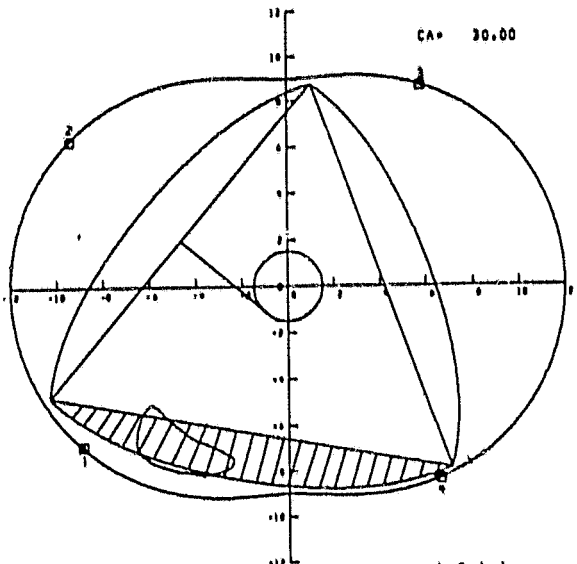


Rotor Position at the Beginning of Intake

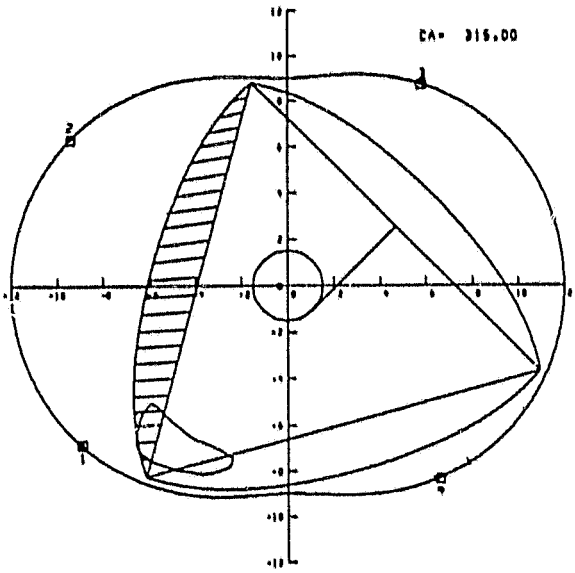


Rotor Position at the Start of Compression

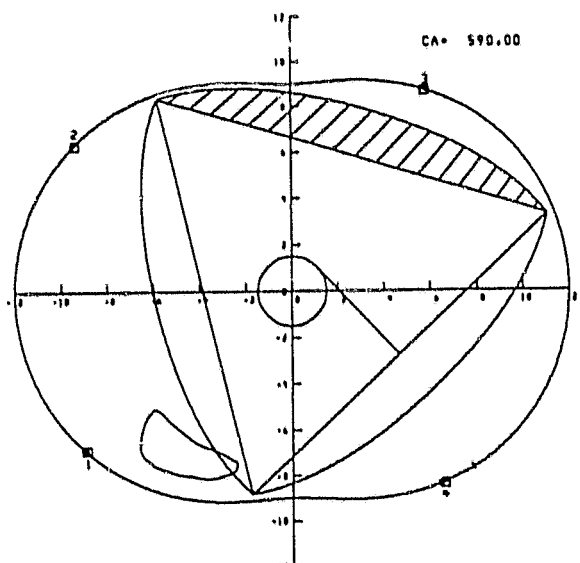


Rotor Position Early in Expansion Stroke

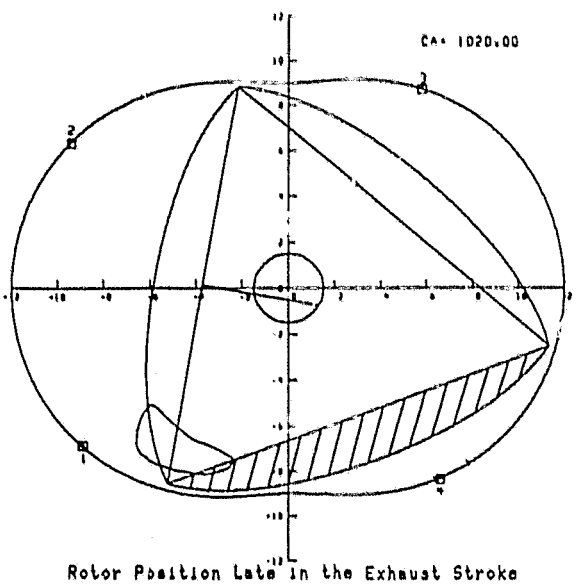


Rotor Position Late in the Exhaust Stroke

Figure 1. - Illustration of 4-stroke cycle for the rotary engine (Wankel configuration).

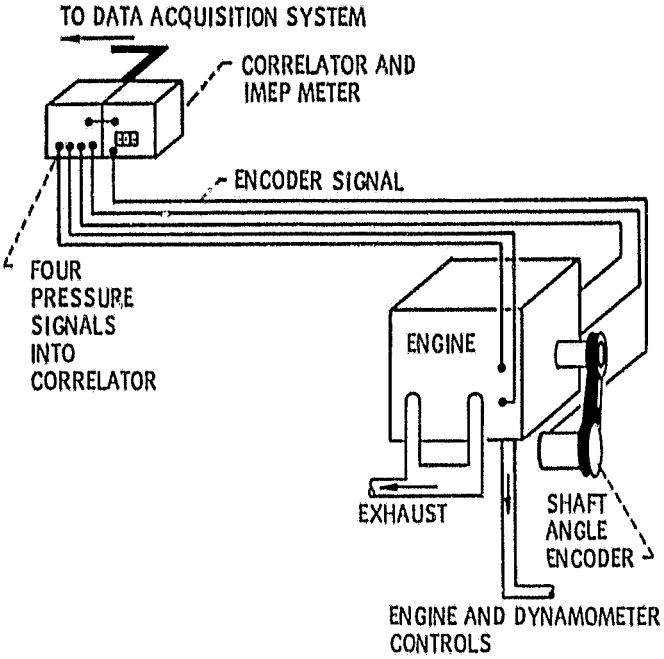


Figure 2. - Test configuration.

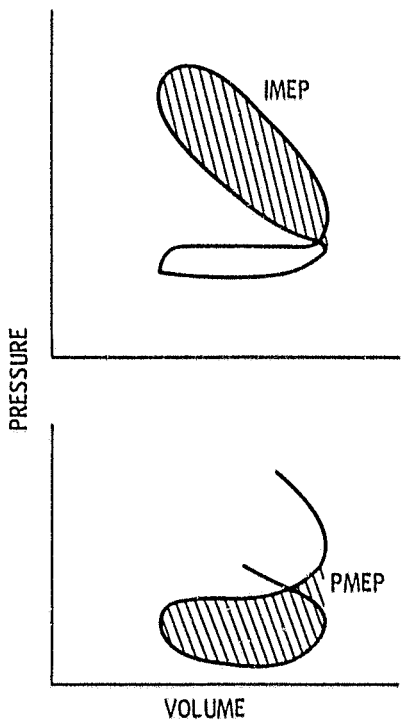


Figure 3. - Definition of IMEP and PMEP.

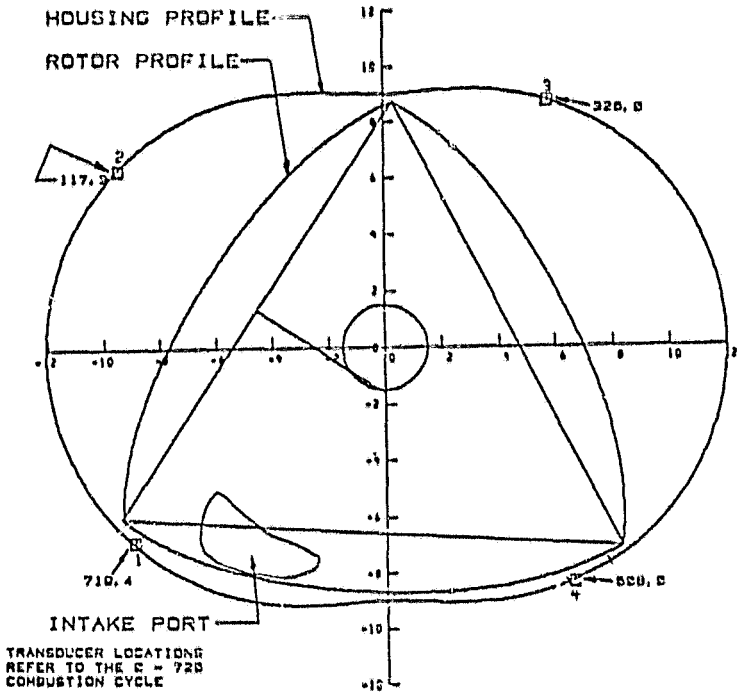


Figure 4. - Transducer locations.

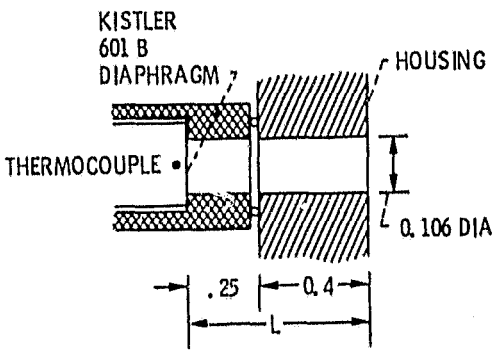


Figure 5. - Transducer installation in rotor housing.

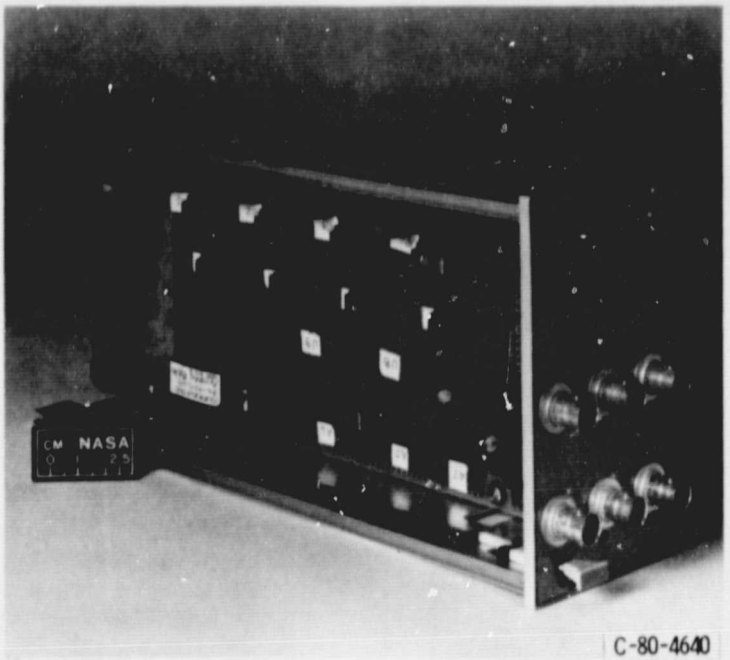


Figure 6. - Photograph of signal correlator.

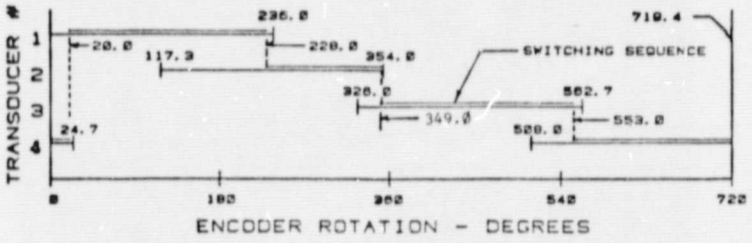


Figure 7. - Transducer active regions.

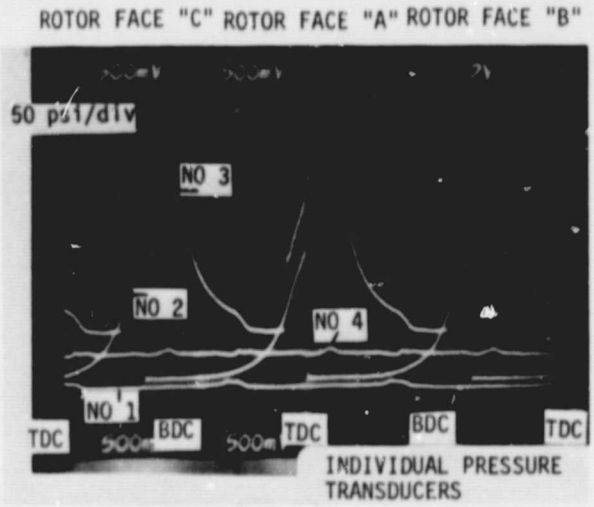


(a)

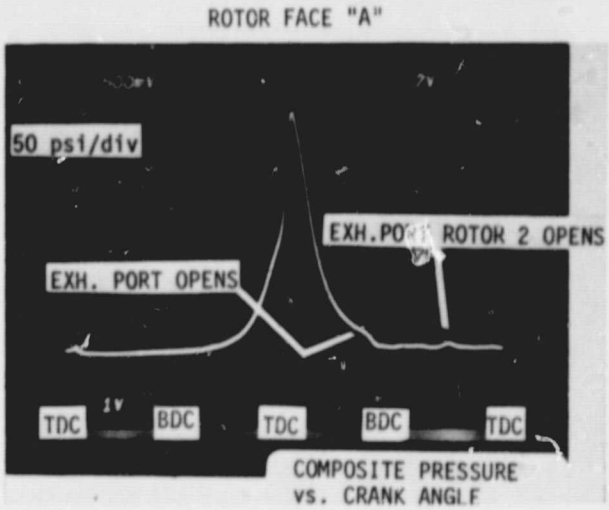


(b)

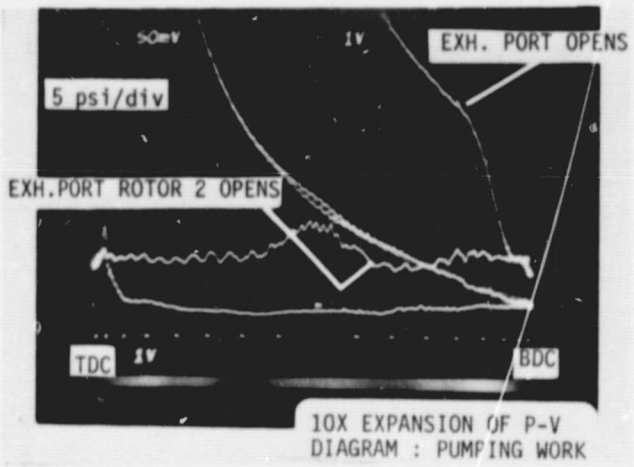


(c)

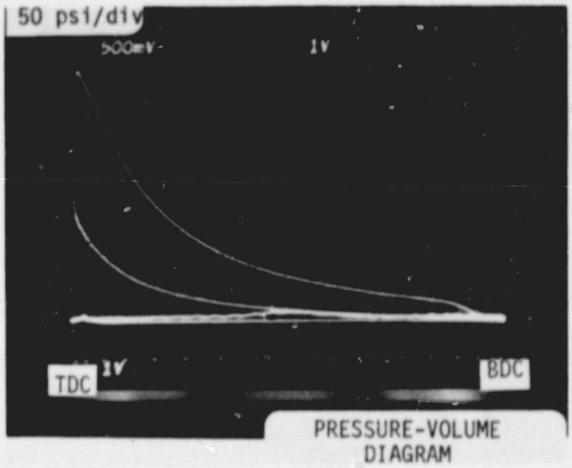


(d)

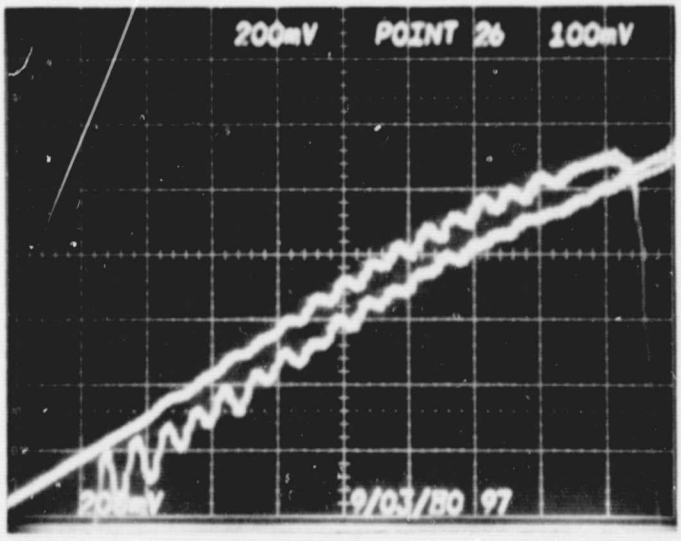


(e)

Figure 8. - Transducer and signal correlator outputs. Engine condition 2000 RPM, 38 ft-lbf, $\Phi$ = .88.

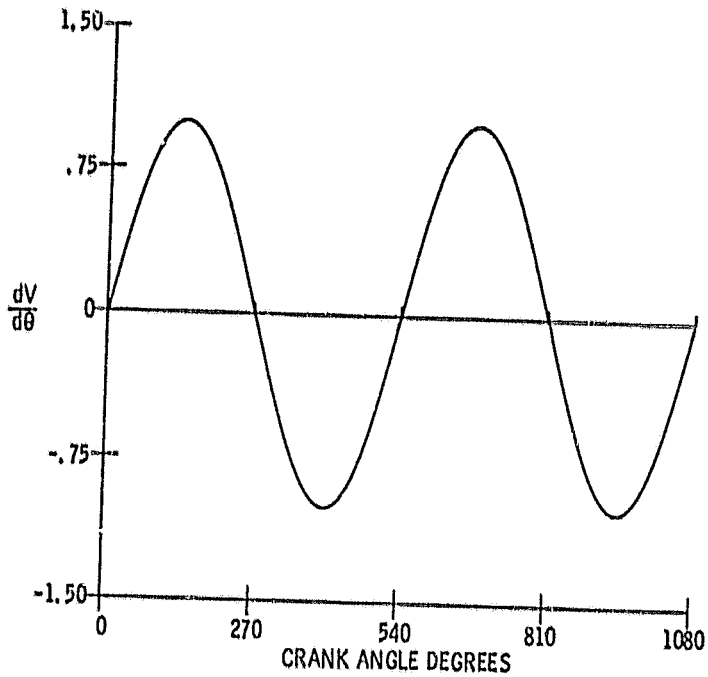


Figure 9. - Rate of change of volume with crank angle.

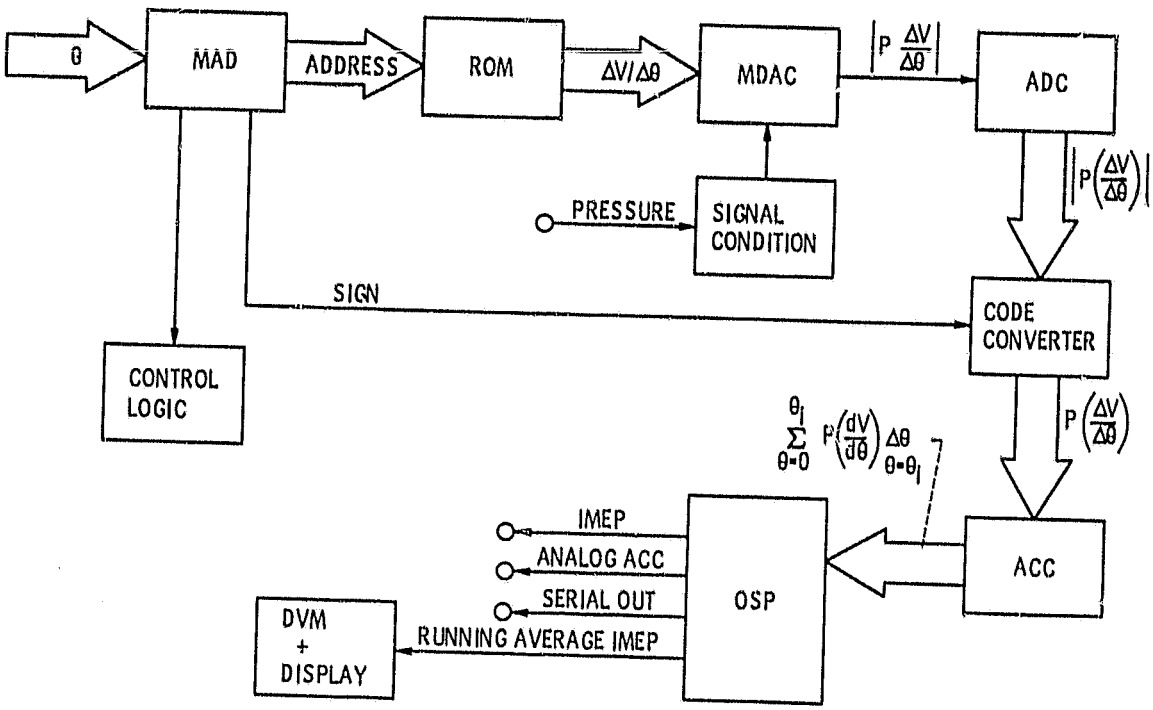


Figure 10. - Block diagram of IMEP measurement system.

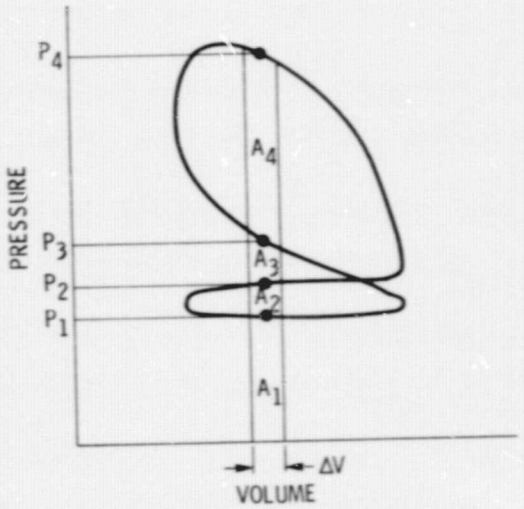


Figure 11. - Computational slice used by IMEP instrument.

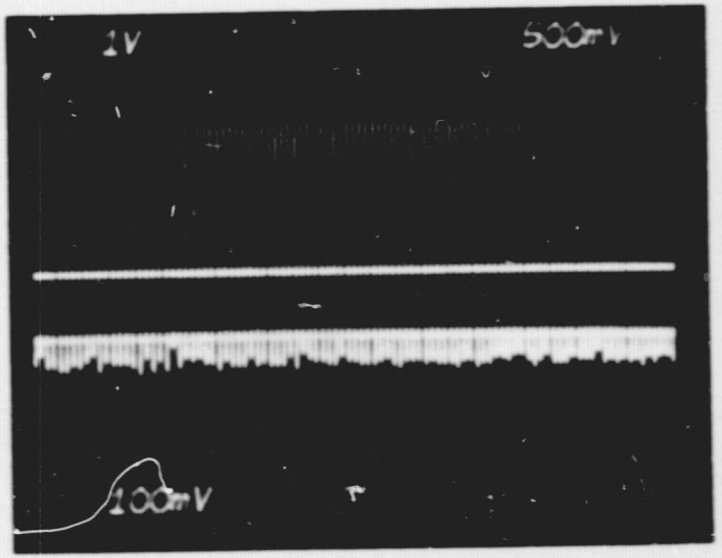


(a) TYPICAL BARGRAPH OF IMEP AND PMEP AT CONSTANT SPEED AND LOAD.

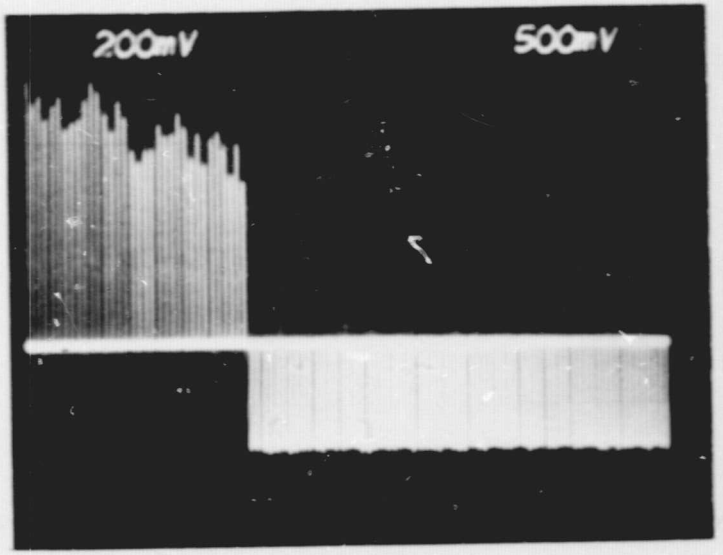


(b) TRANSITION IN PER CYCLE IMEP FROM FIRING TO MOTORING.

Figure 12.

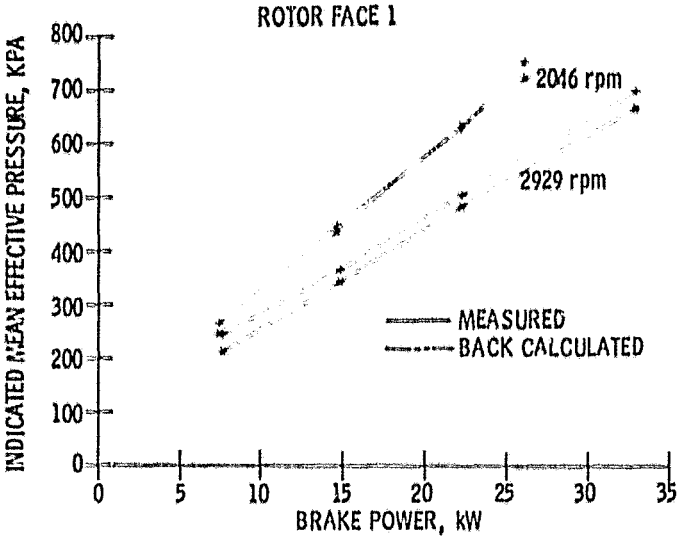


Figure 13. - Back calculation of IMEPT and measured IMEPT versus power.

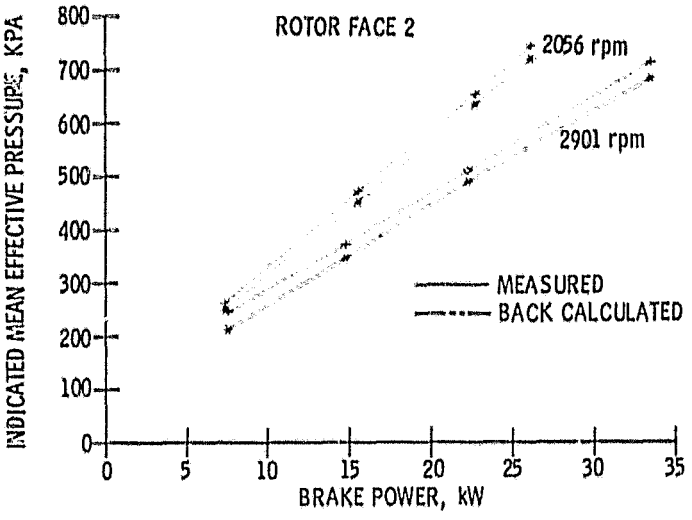


Figure 14. - Back calculation of IMEPT and measured IMEPT versus power.

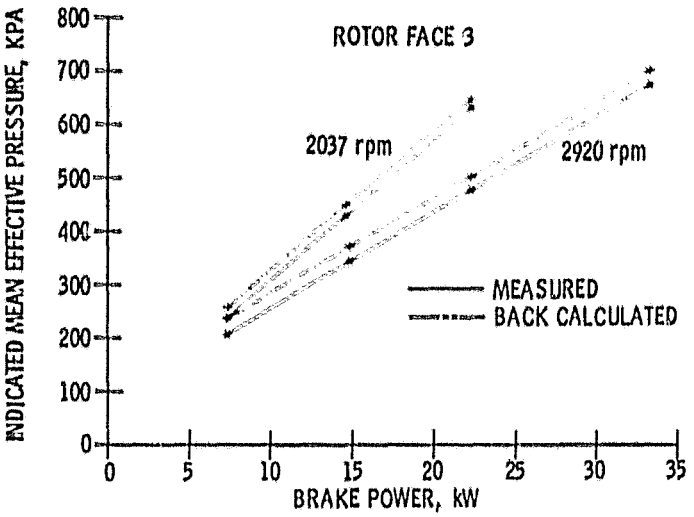


Figure 15. - Back calculation of IMEPT and measured IMEPT versus power.

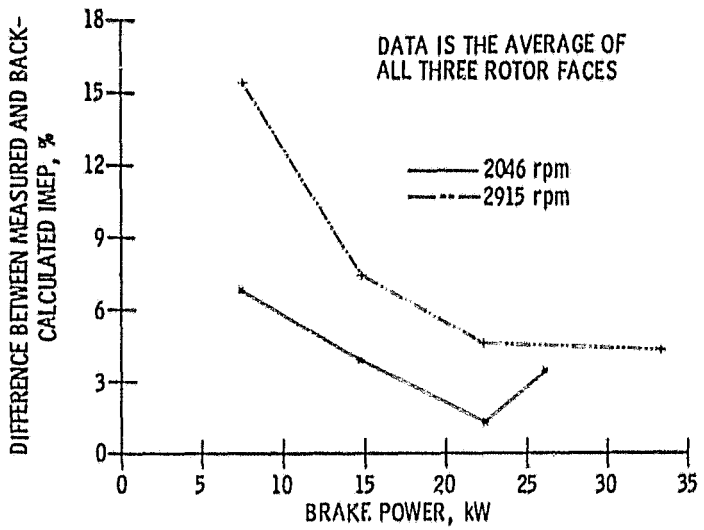


Figure 16. - Average error in IMEPT measurements.

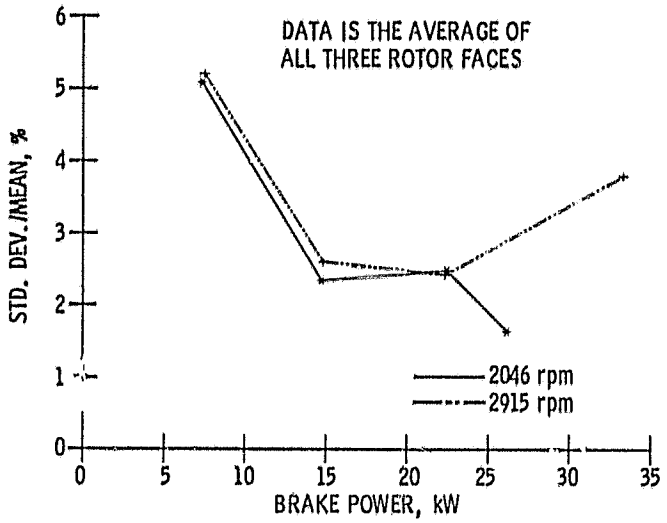


Figure 17. - Average variability in 100 cycle IMEPT measurements.

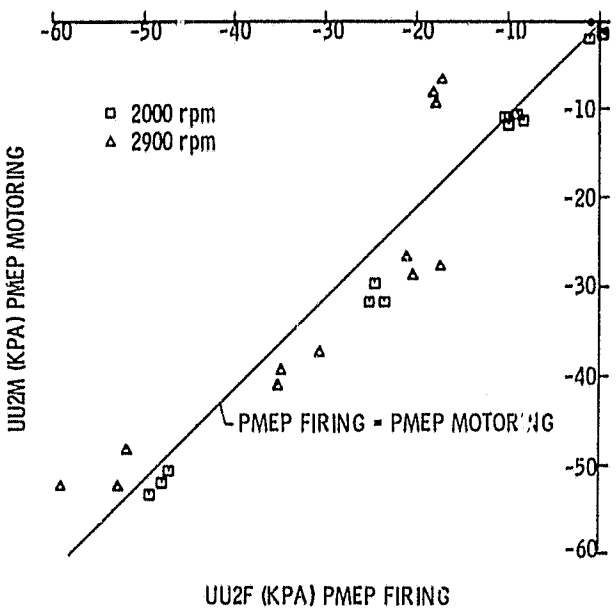


Figure 18. - PMEP firing versus PMEP motoring.

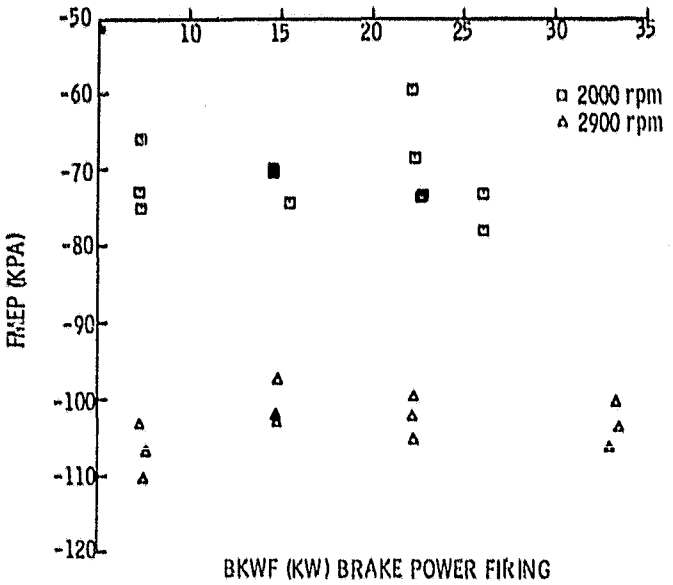


Figure 19. - FMEP versus brake power.